scientific reports

Check for updates

OPEN

Proton- compared to X-irradiation leads to more acinar atrophy and greater hyposalivation accompanied by a differential cytokine response

Inga Solgård Juvkam[1,2], Olga Zlygosteva[3], Mateusz Sitarz[4], Brita Singers Sørensen[4,5], Hans Christian D. Aass[6], Nina Jeppesen Edin[3], Hilde Kanli Galtung[1], Tine Merete Søland[1,7,8] & Eirik Malinen[2,3,8]✉

Proton therapy gives less dose to healthy tissue compared to conventional X-ray therapy, but systematic comparisons of normal tissue responses are lacking. The aim of this study was to investigate late tissue responses in the salivary glands following proton- or X-irradiation of the head and neck in mice. Moreover, we aimed at investigating molecular responses by monitoring the cytokine levels in serum and saliva. Female C57BL/6J mice underwent local fractionated irradiation with protons or X-rays to the maximally tolerated acute level. Saliva and serum were collected before and at different time points after irradiation to assess salivary gland function and cytokine expression. To study late responses in the major salivary glands, histological analyses were performed on tissues collected at day 105 after onset of irradiation. Saliva volume after proton and X-irradiation was significantly lower than for controls and remained reduced at all time points after irradiation. Protons caused reduced saliva production and fewer acinar cells in the submandibular glands compared to X-rays at day 105. X-rays induced a stronger inflammatory cytokine response in saliva compared to protons. This work supports previous preclinical findings and indicate that the relative biological effectiveness of protons in normal tissue might be higher than the commonly used value of 1.1.

Keywords Protons, X-rays, Fractionated irradiation, Mice, Salivary glands, Cytokines

Head and neck cancer (HNC) is the sixth most common cancer in the world, and treatment typically involves surgery followed by radiotherapy (RT) or chemoradiotherapy[1,2]. RT may damage normal tissue surrounding the tumour, thereby causing detrimental late toxicities which might impair the patient's quality of life. A common late toxicity for HNC patients is hyposalivation caused by RT-induced damages to the salivary glands[3,4]. Reduced saliva production has detrimental effects on oral health causing loss of taste, difficulties in speaking, eating, and swallowing, accompanied by increased incidence of caries and fungal infections[3,5]. Hyposalivation is often, but not always, associated with xerostomia, the patient-reported sensation of having a dry mouth[6,7]. Therefore, approaches that can reduce the radiation dose to salivary glands and thus potentially decrease related toxicities are warranted.

Proton therapy is an important tissue-sparing modality due to its favourable dose distribution compared to conventional X-ray therapy. With protons, a large part of the total dose will be deposited in a steep and localised region, called the Bragg peak, with less entrance dose compared to X-rays and practically no exit dose[8]. X-rays on the other hand will travel through the entire cross-section of the patient and deposit dose along the whole

[1]Institute of Oral Biology, Faculty of Dentistry, University of Oslo, Oslo, Norway. [2]Department of Radiation Biology, Institute of Cancer Research, Oslo University Hospital, Oslo, Norway. [3]Department of Physics, Faculty of Mathematics and Natural Sciences, University of Oslo, Oslo, Norway. [4]Danish Centre for Particle Therapy, Aarhus University Hospital, Aarhus, Denmark. [5]Department of Experimental Clinical Oncology, Aarhus University Hospital, Aarhus, Denmark. [6]The Blood Cell Research Group, Department of Medical Biochemistry, Oslo University Hospital, Oslo, Norway. [7]Department of Pathology, Oslo University Hospital, Oslo, Norway. [8]Joint senior authors ✉email: eirik.malinen@fys.uio.no

beam path[9]. Compared to X-ray therapy, proton therapy will thereby lead to reduced normal tissue dose and potentially less toxicities. However, the clinical documentation of reduced tissue toxicity after protons in HNC is still quite sparse[10], and HNC patients still report xerostomia after proton therapy[11,12].

Compared to irradiation with X-rays, proton irradiation has shown differences in DNA damage and repair[13–17], gene expression modulation[18–23], and inflammatory cytokine production[24]. Protons are biologically more effective in killing cells than X-rays, which is commonly implemented in proton therapy clinics as a relative biological effectiveness (RBE) of 1.1[25,26]. The standard RBE of 1.1 for protons has recently been debated[27–29], as research documenting a variable RBE across the proton beam path is increasing[30–32]. An extensive review has reported an average RBE for cell survival of 1.1 in the entrance region and up to 1.7 at the distal fall-off of the Bragg peak[33]. The variable RBE is suggested to be in part caused by the increase in linear energy transfer (LET) as the protons slow down towards the Bragg peak[26,34]. This increase in LET at the distal fall-off of the Bragg peak has shown to have clinical implications to normal tissues located close to the tumour[35–39]. The response of normal tissues to proton irradiation is still largely unknown, despite the established differences between protons and X-rays. Therefore, there is a requirement for further preclinical experiments to investigate this matter. Also, monitoring changes in cytokine levels after radiotherapy is important to understand the evolution of systemic signals and association between inflammatory responses, the immune system, and the development of normal tissue toxicities[40]. Thus, there is a need for systematic comparisons of cytokine production and late normal tissue responses occurring after proton- and X-irradiation.

In the present study, we investigate functional, cellular, and structural changes in mouse salivary glands after fractionated proton or X-irradiation in vivo. For protons, we use two approaches that give different irradiated volume, dose- and LET-distributions in the mouse head. The first proton approach (transmission mode: TM) has a similar dose distribution, LET, and irradiated volume as the corresponding X-ray group[41]. The second proton approach (Bragg peak: BP) has a more clinically relevant dose distribution than TM, with the Bragg peak ending up in the middle of the mice where normal tissues at the distal fall-off of the Bragg peak might receive high LET protons. Moreover, we study molecular responses by monitoring the cytokine levels in serum and saliva at different time points before and after irradiation and link the levels with the observed normal tissue responses. Through this, we bring new light on tissue and systemic effects after proton therapy of the head and neck.

Results

Decreased saliva volume after protons versus X-rays at day 105

To investigate the salivary gland function after proton or X-ray therapy, saliva volume was collected before and at several different time points after irradiation. Saliva volume was significantly reduced after X- or proton irradiation compared to controls right after treatment termination (day 9 for protons, day 12 for X-rays) and at day 35, 70, and 105 after onset of fractionated irradiation (Fig. 1). The BP group showed a tendency of higher saliva volume compared to the TM group at every time point after irradiation. The TM and X-ray group showed similar saliva levels except at day 105, where the TM group showed significantly lower saliva volume compared to the X-ray group ($p = 0.043$), even though the TM group received 45 Gy in total dose while the X-ray group received 65 Gy.

Loss of acinar cells, increased salivary gland fibrosis, and reduced gland size in irradiated groups

To investigate the salivary gland damage at day 105 after onset of fractionated irradiation, histological evaluations were performed using hematoxylin and eosin (HE), alcian blue (AB), and Masson trichrome (MT) staining. HE-

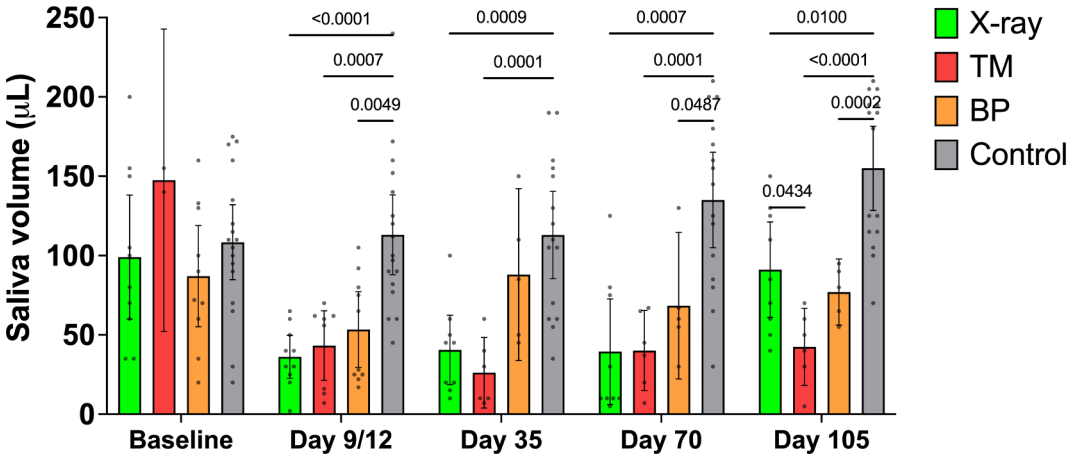

Fig. 1. Reduced saliva volume in irradiated groups. Saliva volume in all treatment groups before irradiation (baseline), right after treatment termination (day 9 for protons, day 12 for X-rays), and at different time points after irradiation (days 35, 70, and 105). P-values are shown only between groups with $p \leq 0.05$. Data are presented as mean ± 95% CI. TM = transmission protons, BP = Bragg peak protons.

stained sections showed atrophy of acinar cells in the submandibular (SMG) and the sublingual salivary gland (SLG) in all three irradiated groups (Fig. 2). Conversely, in the parotid gland (PG) acinar atrophy was only observed in the TM group. In the TM mice, acinar atrophy was observed in the entire SMG and SLG. In BP and X-ray mice, however, acinar atrophy was only observed in focal areas of the SMG and SLG, consistent with lower saliva volume observed in the TM mice at day 105. No acinar atrophy was observed in any of the control glands. AB-stained sections showed less cells stained blue in all irradiated groups, indicating fewer cells containing mucin (acinar cells) compared to controls (Fig. S1), confirming the observation made in HE-stained sections. Analysis of total gland area showed significantly reduced SMG area in the X-ray and TM group (X-ray: $p = 0.0415$, TM: $p = 0.003$) (Fig. 3A-B), with TM mice demonstrating the largest reduction compared to controls. The same tendency was observed in SLG, but it was not statistically significant. Analysis of the amount of fibrotic area was performed using MT-stained sections. Both proton groups demonstrated a significant increase in fibrotic area compared to controls (TM: $p = 0.002$, BP: $p = 0.011$). The X-ray group did not display a difference in fibrotic area compared to the controls (Fig. 3C-D).

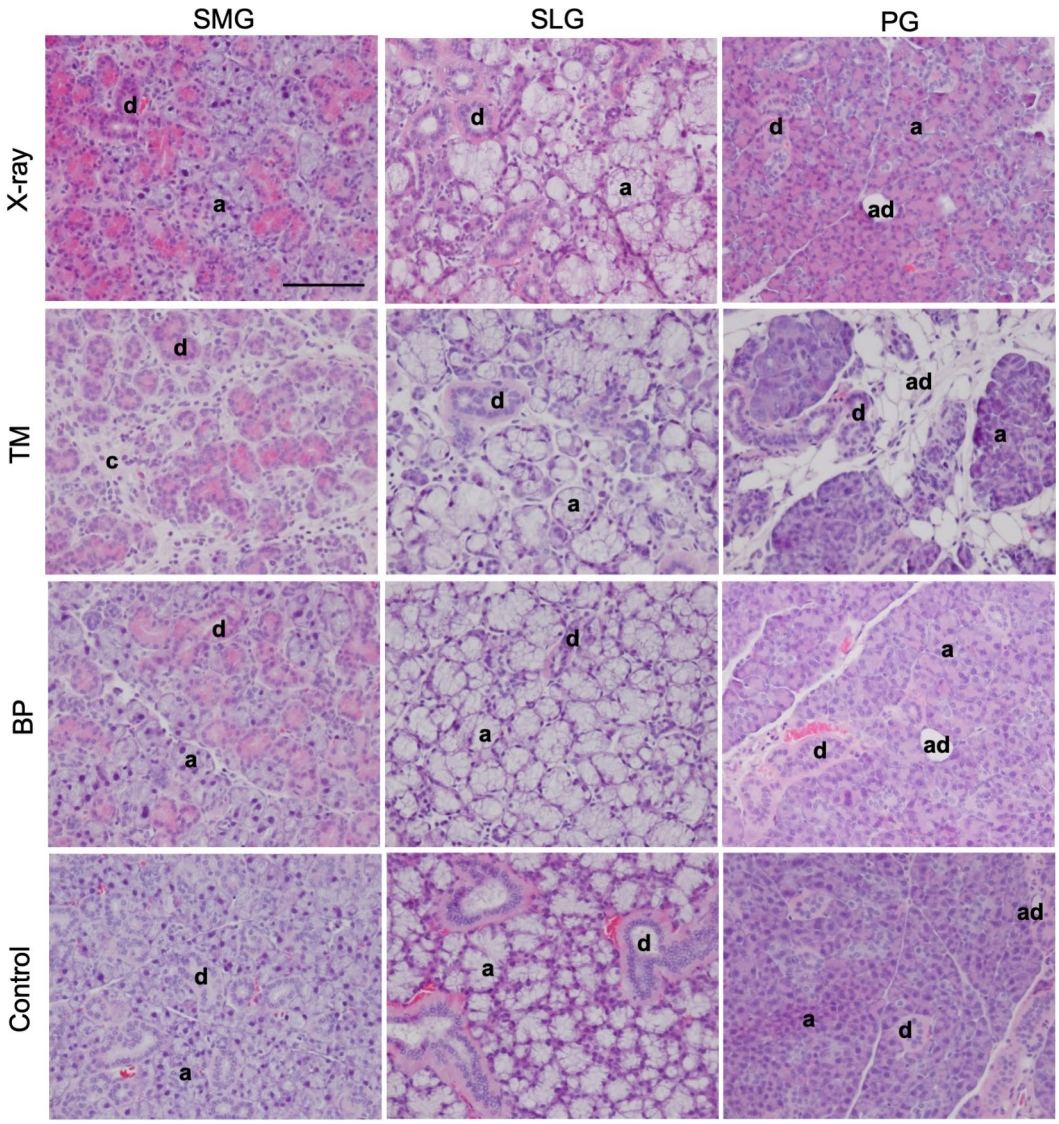

Fig. 2. Acinar atrophy was observed in all irradiated groups. Representative images of hematoxylin and eosin (HE) stained sections 105 days after onset of proton (TM and BP) or X-irradiation. HE-sections of irradiated and control submandibular (SMG), sublingual (SLG) and parotid (PG) glands. Acinar atrophy was observed in all irradiated groups of SMG and SLG. In the TM mice, acinar atrophy was observed in the entire SMG and SLG, while in BP and X-ray mice acinar atrophy was only observed in parts of the SMG and SLG. No areas of acinar atrophy were observed in any of the control glands. The images were taken with a 20x objective and the scale bar is 100 µm. TM = transmission protons, BP = Bragg peak protons, a = acinar cells, d = ducts, c = connective tissue, ad = adipocytes.

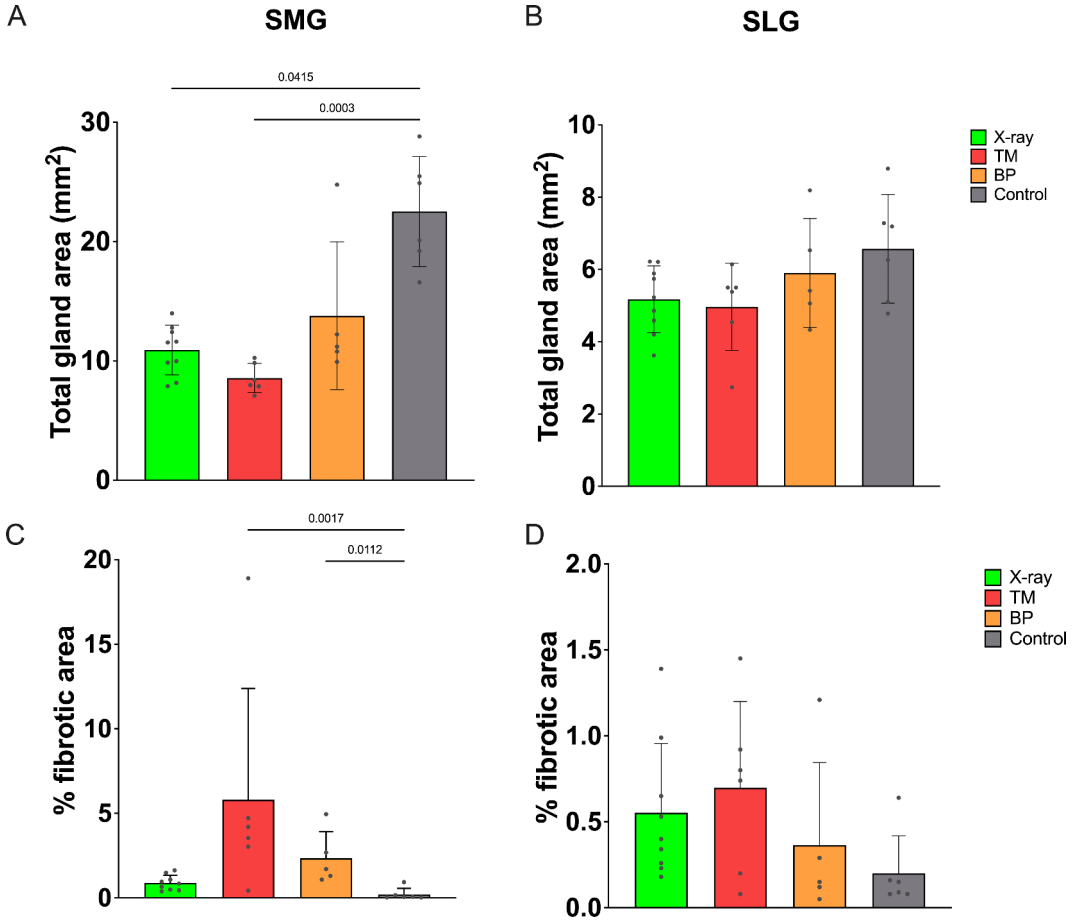

Fig. 3. Total gland area and fibrotic area. Quantified total gland area of the (**A**) submandibular gland (SMG), and (**B**) the sublingual gland (SLG) in all treatment groups and controls at day 105. Percentage of fibrotic area in (**C**) SMG, and (**D**) SLG in all treatment groups and controls at day 105. P-values are shown only between groups with $p \leq 0.05$. Data are presented as mean ± SD. TM = transmission protons, BP = Bragg peak protons.

Significantly less acinar cells after protons compared to X-rays at day 105

To further assess the acinar atrophy observed in the HE-stained sections, immunofluorescence labelling using antibodies against the acinar cell marker MIST1 and the ductal cell marker CK19 was performed (Fig. 4A-B). This showed a significant reduction of MIST1$^+$ nuclei relative to total nuclei in all irradiated groups compared to controls (Fig. 4C), confirming our observation of loss of acinar cells in HE-stained sections. Interestingly, both proton groups showed a significantly lower percentage of MIST1$^+$ nuclei compared to the X-ray group (TM: $p < 0.0001$, BP: $p = 0.0214$). The largest reduction in MIST1$^+$ nuclei was found in the TM group, correlating well with the largest increase of fibrotic area, largest reduction of total gland area and lowest saliva volume in this group. The cell density was not different between any of the treatment groups (Fig. 4D). Surprisingly, we observed more CK19$^+$ cells in the irradiated sections, especially in areas with a low number of MIST1$^+$ nuclei, as shown in Fig. 4B. Moreover, HE- and AB-stained sections of the SMG showed more clusters of large acinar cells in both proton groups compared to the X-ray group. Immunofluorescence showed that these acinar cell clusters were expressing MIST1 (Fig. S2), indicating that they might still have a secretory phenotype.

Cytokine profiles after proton versus X-ray fractionated irradiation

A panel of 11 cytokines were assessed in both serum and saliva. Of these, four cytokines (IL-1α, G-CSF, TIMP-1, and MIP-1α) were commonly detected in saliva and serum samples after both proton and X-irradiation (Fig. 5 and S3), while one (TNF) was only detected in saliva. Most often, irradiation caused increased levels of all detected cytokines. In saliva samples, the levels of G-CSF, TNF, TIMP-1, and MIP-1α were significantly increased in the X-ray group compared to controls at day 9/12, while the increase in IL-1α level was not significant (Fig. 5). In addition, the levels of IL-1α, TIMP-1 and TNF were significantly higher in the X-ray group compared to both proton groups at day 9/12, while the levels of G-CSF and MIP-1α were significantly higher for the X-ray group compared to the TM group only. At later time points, the X-ray group showed a significant increase in IL-1α and TNF levels at day 70 and a similar trend in G-CSF and MIP-1α (not significant). TIMP-1 levels were also increased in all irradiated groups compared to controls at days 70 and 105 (significant for X-ray and BP groups). In serum samples, the levels of IL-1α were significantly higher in the X-ray group compared to both proton groups, while it was opposite for G-CSF levels measured at day 9/12 (Fig. S3). The levels of TIMP-1 were

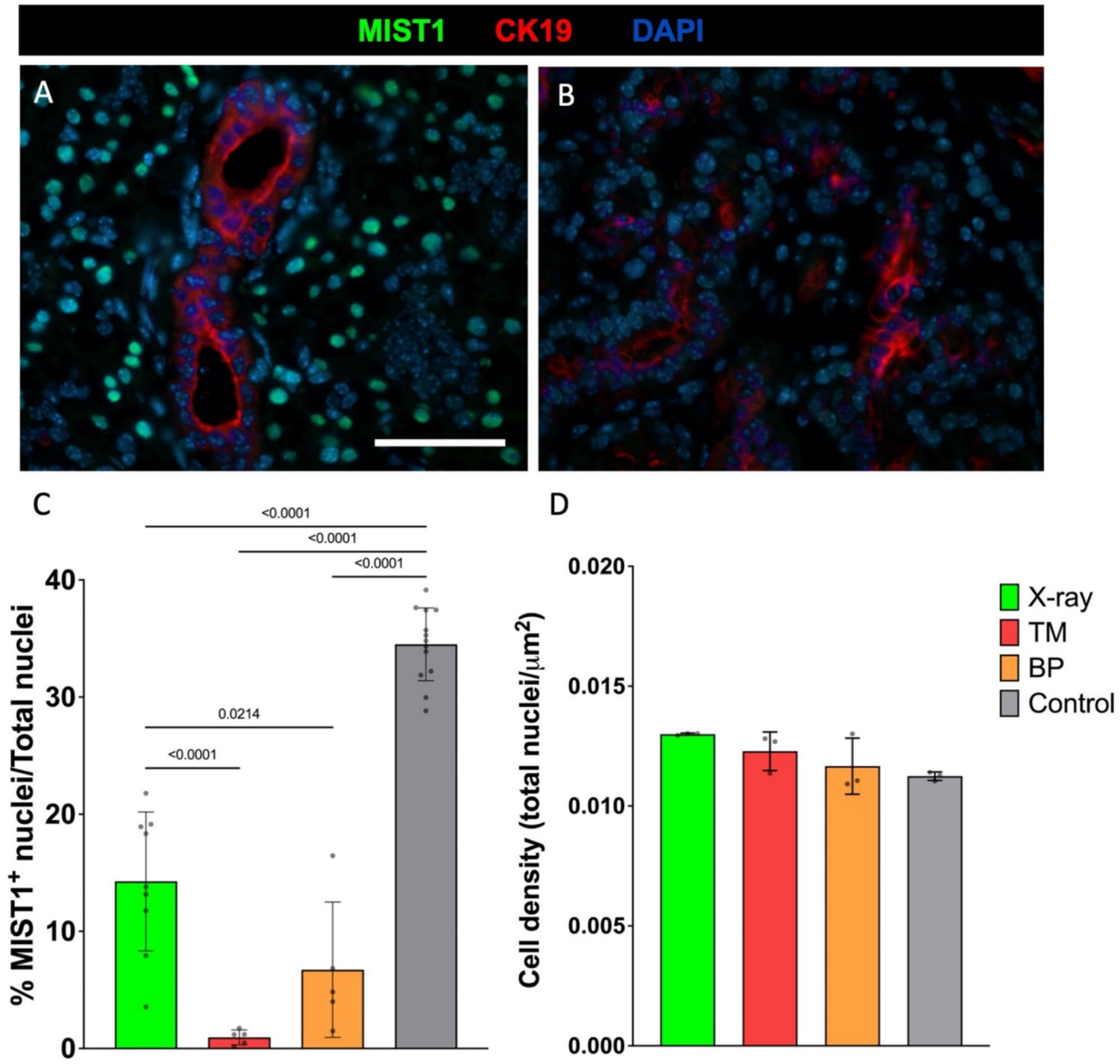

Fig. 4. Reduced number of acinar cells in all irradiated groups showed by the acinar cell marker MIST1 and the ductal cell marker CK19 in the submandibular gland (SMG). (**A**) A representative immunofluorescence image showing a control SMG section with several MIST1$^+$ nuclei (green) and two CK19$^+$ ducts (red), and (**B**) a representative immunofluorescence image showing an irradiated SMG section with no MIST1$^+$ nuclei and an increased expression of CK19$^+$ cells. Images were taken with a 40x objective and the scale bar is 50 μm. (**C**) MIST1$^+$ nuclei relative to the total number of nuclei in each treatment group. P-values are shown only between groups with $p \leq 0.05$. (**D**) Cell density (total nuclei/ μm^2) in each treatment group. Data are presented as mean ± SD. TM = transmission protons, BP = Bragg peak protons.

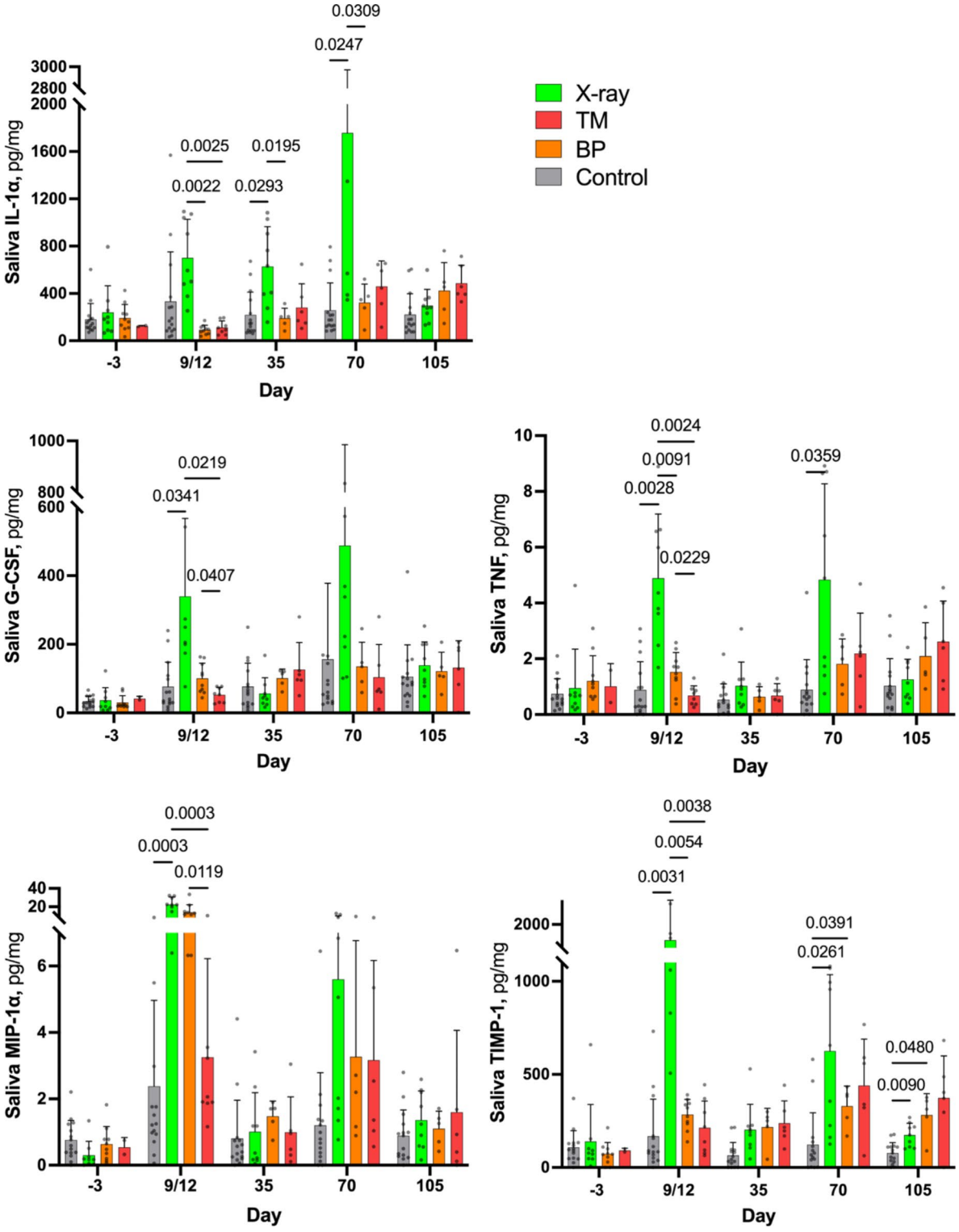

Fig. 5. Salivary cytokines. Levels of salivary cytokines before and after fractionated irradiation at days − 3, 9/12, 35, 70 and 105. P-values are shown only between groups with $p \leq 0.05$. Data are presented as mean ± SD pg/ml cytokine per total protein mg/ml. TM = transmission protons, BP = Bragg peak protons.

significantly increased in the TM group compared to the BP and X-ray groups at day 9/12 and 70, and also compared to the X-ray group at day 105.

Discussion

Proton therapy is expected to reduce normal tissue toxicity compared to conventional X-ray therapy. However, there are still knowledge gaps regarding differences in normal tissue responses between protons and X-rays. In the present work, late tissue responses in a mouse model were investigated, with the main focus being cellular, structural, and functional changes of the salivary glands after proton- or X-irradiation. To our knowledge, this is the first study making such a comparison. At the time of termination (day 105), we found more pronounced hyposalivation after proton irradiation (TM group), indicating that protons are more effective at causing this endpoint. Moreover, we found significantly fewer acinar cells and a tendency towards greater gland size reduction and more fibrosis in the SMG irradiated by protons. All of these differences were found even though the total physical dose was lower in the two proton groups compared to the X-ray group (TM protons: 45 Gy, BP protons: 41 Gy, X-rays: 65 Gy).

In a previous study, we investigated early tissue responses after proton or X-irradiation of the mouse head and neck[41]. In that work, protons gave a stronger response in terms of acute mucositis. In the present study, we examined late tissue responses in the same cohort of mice. Again, proton irradiation gave stronger tissue responses in the salivary glands. Two different proton irradiation approaches were used to evaluate different aspects of proton therapy. In the first approach (TM), protons with rather high energies were used, resulting in the Bragg peak being deposited behind the mouse head. This approach was designed to mirror the dose distribution of the corresponding X-ray treatment, with a gradually decreasing dose throughout the animal (Fig. 6A; for further dosimetry and Monte Carlo simulations of the dose, see[41]). The TM approach was employed to directly compare the biological effectiveness of protons and X-rays without a difference in irradiated volume and depth-dose distribution. In the second approach (BP), the Bragg peak was deposited at the midline of the mouse head. This approach was designed to mimic a clinical situation where normal tissues located right behind the tumour are at risk of receiving high LET protons. Thus, the TM and BP approaches yield different irradiated volume, dose- and LET distributions, as evident in our previous study[41]. An important finding from the present work was that the TM approach gave more pronounced tissue effects compared to the BP approach, indicating that irradiated volume is more important than LET for protons. However, the TM animals received 45 Gy total dose while the BP animals received only 41 Gy in total dose which may have impacted the result.

Adult salivary gland homeostasis seems to depend mainly on lineage-restricted progenitor cells[5,42,43]. However, after injury, there is evidence pointing towards induced plasticity between the different cell compartments of the salivary glands, where ductal cells can give rise to new acinar cells. This has been observed after severe duct ligation in mice[44], after irradiation in mice[45], and at late time points after irradiation in HNC patients[46]. In the present study, we observed an increase of $CK19^+$ duct cells, especially in areas with a low number of $MIST1^+$ acinar cell nuclei. Thus, our results point towards an increase of duct cells and an accompanying loss of acinar cells in irradiated glands, and therefore support the hypothesis regarding non-lineage restricted plasticity. Although a general loss of acinar cells was identified in the irradiated glands in our work, some large acinar cell clusters were still present at day 105 after irradiation. This observation was more frequent in the two proton groups compared to the X-ray group. These acinar cell clusters were $MIST1^+$, which also has been observed in HNC patients more than 10 years after radiotherapy[46], where it was suggested that they might thus still have a secretory phenotype. MIST1 is known to induce and maintain the secretory phenotype also in pancreatic acinar cells[47], and induce the expression of salivary amylase[48]. Due to the large loss of acinar cells in the rest of the gland, the acinar cell clusters are not sufficient to maintain proper salivary gland function, confirmed by the observed hyposalivation at day 105.

Different expressions of cytokines after proton- compared to X-irradiation have previously been shown in plasma[24] and in vitro[49]. To our knowledge, there is no other study comparing salivary cytokines after proton and X-ray therapy, neither in a clinical nor in a preclinical setting. We have previously argued that salivary cytokines are more relevant than serum cytokines for assessing associations with late tissue responses in salivary glands[50]. Radiation-induced changes in expression levels in saliva might be more prominent compared to those in serum because the local radiation field covers mostly the oral cavity and salivary glands. In the current work, we also included cytokines in serum as little is generally known about differential systemic responses after proton- compared to X-irradiation. We found that the levels of IL-1α in serum and saliva, and TNF in saliva showed significant increase after exposure to X-rays compared to protons and controls. This was displayed as a wave immediately after irradiation and at day 70. IL-1α and TNF have been reported to drive the inflammatory radiation response[51]. All other detected cytokines in saliva also showed increased levels after X-rays compared to protons at day 9/12 and 70. However, protons also gave a slightly upregulated expression pattern in saliva for many cytokines compared to controls, but the increase was often not significant. For later time points, TIMP-1 in saliva showed an increase in all irradiated groups compared to controls, with higher levels in the TM group compared to the X-ray group at day 105. TIMP-1 has been implicated in fibrosis development[52] and the TM group indeed demonstrated replacement of glandular tissue with fibrotic tissue at day 105 compared to the BP and X-ray groups.

The G-CSF level in serum was greatly increased after proton- compared to X-irradiation at day 9/12. This might be connected to a systemic inflammatory response caused by more severe radiation-induced early effects after proton irradiation. In our previous study comprising the same animals, protons induced more severe oral mucositis compared to X-rays[41]. G-CSF plays a role in controlling the immune response, preventing overactivation of lymphocytes by reducing pro-inflammatory mediators but at the same time stimulating neutrophil recruitment[53]. In fact, oral G-CSF administration has been suggested to combat oral mucositis[54]. Thus, the high acute level of G-CSF after proton irradiation implies that there might be a rapid modulation of

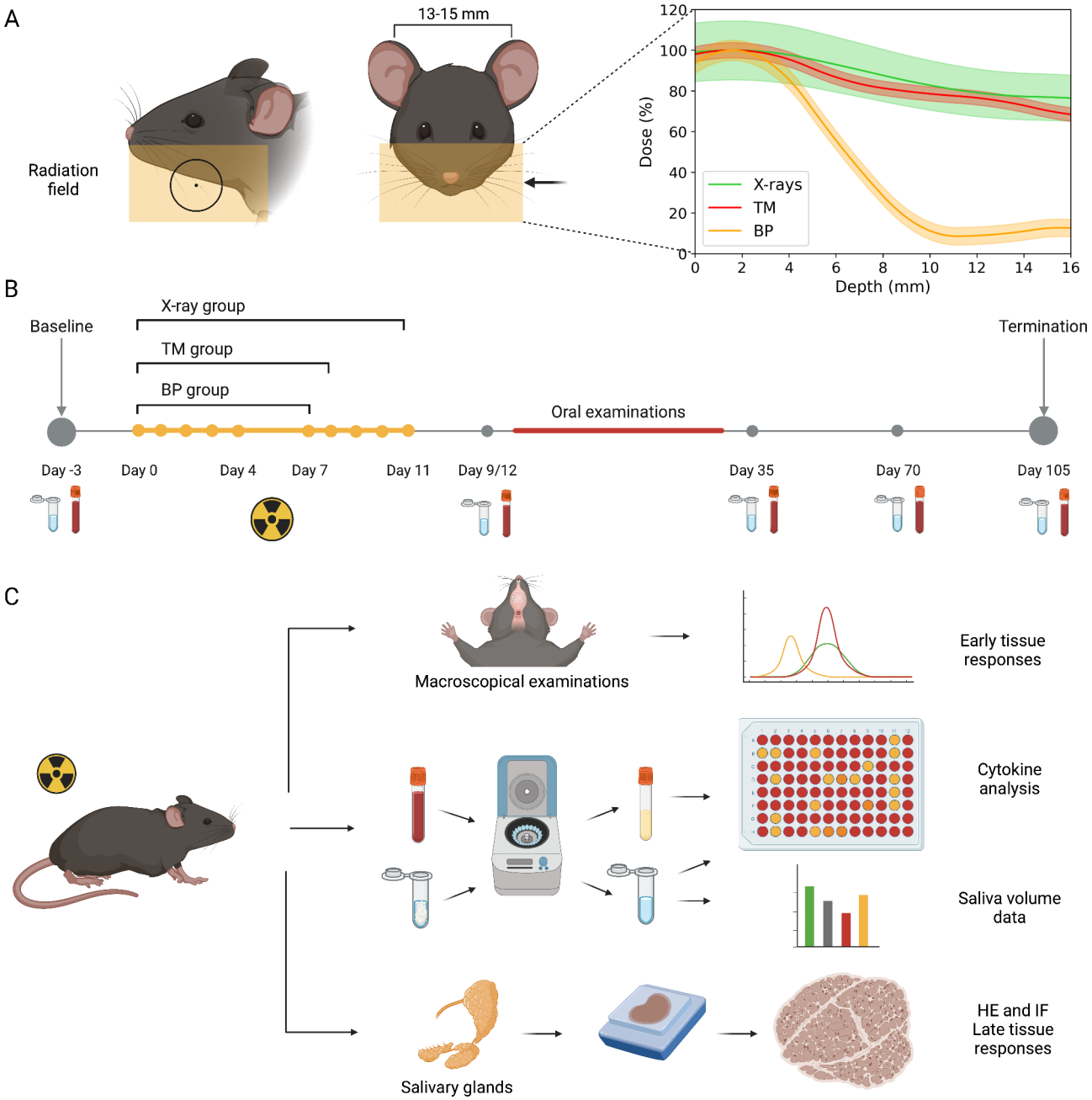

Fig. 6. Experimental set-up. Radiation field and dosimetry (**A**), timeline (**B**) and graphical overview (C) of the X-ray and proton experiments. In (**A**), the radiation field size was identical for all irradiation groups, and covered the oral cavity, pharynx, and the major salivary glands. The depth-dose curves shown (including 1-sigma uncertainty) are re-analysed alanine dosimetry data from[41], including normalization and cubic spline interpolation across the mouse head. In (**B**), examinations of the oral cavity were performed during the early phase (days 0–35) and have been published elsewhere[41]. TM = transmission mode proton treatment plan, BP = Bragg peak proton treatment plan, HE = hematoxylin and eosin staining, IF = immunofluorescence labelling. Figure created with Biorender.com.

the immune response that potentially could impact and lower the systemic expression of other inflammatory cytokines. As X-rays causes higher G-CSF levels compared to protons in saliva, this may indicate that the response in salivary glands differs from the rest of the irradiated tissues in the mouse head and neck. Additionally, the total dose may be considered as a factor that influences the cytokine response as the proton groups received lower dose than the X-ray group. However, the increased cytokine response after X-rays is not proportional to the dose difference.

A limitation of this study is that the proton and X-ray experiments were performed at two different facilities due to the lack of an operational proton therapy centre in Oslo, Norway. Therefore, the proton experiments

were performed in Aarhus, Denmark while the comparative X-ray experiment was performed in Oslo, Norway. This can potentially cause unknown differences in the mice, e.g. due to different microbiological backgrounds. However, we used the same animal vendor, mice strain, and age of mice to reduce the differences as much as possible. In addition, we incorporated control animals in both experiments, and we did not observe any differences between the proton controls and the X-ray controls. Finally, the use of gel-like food during the acute recovery phase could have affected the salivary gland function in the irradiated animals.

Taken together, the results of the current study indicate that proton irradiation causes more severe late tissue responses in the salivary glands compared to X-irradiation, even with lower total doses. We demonstrate more extensive salivary gland damage and subsequently larger salivary gland dysfunction after proton irradiation, at least with the TM proton approach. It should be noted, however, that we deliberately irradiated the whole glands (TM and X-ray group). This would not happen in a clinical setting, especially in the case of tissue-sparing proton therapy. Still, our work emphasizes the need to take extra care when planning proton therapy to avoid irradiation of normal tissues as much as possible. Finally, despite the increased damage to the salivary glands after proton irradiation, this was not reflected in the systematically elevated cytokine expression levels in saliva and serum. This indicates that protons and X-rays induce different mechanisms following the primary tissue injury, which warrants further investigation. Future clinical trials comparing proton and X-ray therapy might consider including salivary cytokine analysis to elucidate this difference. The results of this study indicate that the proton RBE for normal tissues in the head and neck, even in front of the Bragg peak, is higher than the current clinical standard of 1.1. This knowledge could impact future proton therapy planning of HNC.

Methods

Animals and ethical considerations

Female C57BL/6J mice from Janvier (France) were kept in a 12-h light/12-h dark cycle under pathogen-free conditions and fed a standard commercial fodder with water given *ad libitum*. At the onset of experiments, animals were 12 weeks old. All animal experiments were performed in accordance with directive 2010/63/EU on the protection of animals used for scientific purposes. Animal experiments conducted in Norway were approved by the Norwegian Food Safety Authority (ID 27931), and experiments conducted in Denmark were approved by the Danish Animal Experiments Inspectorate (ID 2022-15-0201-01146). The authors complied with the ARRIVE guidelines.

Irradiation procedure

Irradiation was performed as previously described[41,55]. The radiation field covered the oral cavity, pharynx, and the major salivary glands[55]. X-irradiation was performed with a Faxitron Multirad225 irradiation system (Faxitron Bioptics, Tucson, AZ, USA) using 100 kV X-rays, 15 mA current, 2.0 mm Al filter, and 0.68 Gy/min dose rate at Oslo University Hospital, Norway. Mice in the X-ray group were irradiated with a total dose of 65 Gy given in 10 fractions over 10 days. Proton irradiation was performed with Varian ProBeam using a pencil beam scanning dedicated nozzle (Varian, Medical Systems, Palo Alto, CA, USA) at the Danish Center for Particle Therapy at Aarhus University Hospital, Denmark. Two different proton treatment groups were included in this study. The first proton treatment group was irradiated with 60 MeV protons to a total physical dose of 44.8 Gy given in 7 fractions over 7 days. Here, the Bragg peak was located outside the mouse (transmission mode, TM) giving this group a similar dose distribution as the X-ray group (Fig. 6A). The second proton treatment group (BP) was irradiated with 25 MeV protons to a total physical dose of 40.8 Gy given in 6 fractions over 6 days, with the distal edge of the Bragg peak located in the middle of the mouse. Delivered doses from X-rays and protons were validated by alanine dosimetry and Monte Carlo simulations, and have previously been published[41]. A new analysis of the dosimetry is now provided in Fig. 6A.

Experimental protocol and study groups

On days 0–4 and 7–11, X-ray or proton fractionated treatment was given once a day to the TM ($n=8$), BP ($n=10$), and X-ray ($n=10$) group (Fig. 6B). Proton controls ($n=7$) and X-ray controls ($n=10$) were sham irradiated under gas anaesthesia (4% Sevoflurane in O_2). During the early phase (days 0–35), mice were monitored daily, and examinations of the oral cavity were performed frequently. Early tissue responses have been published elsewhere[41]. To cope with the early tissue responses, the mice were provided with gel-like food (DietGel Recovery, Clear H2O). This was provided to all the control and irradiated groups together with their regular fodder from day 7–24 upon the first signs of acute oral mucositis and until the mucositis was completely healed in the irradiated animals. Throughout this period, it was observed that the mice ate both the gel and their regular fodder, but to a smaller extent than usual leading to loss of body weight (Fig. S4) correlating with acute mucositis[41,55]. The proton irradiations were terminated earlier than planned due to mouse weight loss (Fig. S4). Several mice in the proton groups reached humane endpoints and were euthanized according to the protocol approved by the national animal authorities. Therefore, the final number of animals at day 105 was as follows: X-rays $n=9$, X-ray controls $n=9$, TM $n=6$, BP $n=5$, proton controls $n=6$. Saliva and blood samples were collected as previously described[41,50,55] at baseline (day −3), right after termination of irradiation (day 9 for the BP and TM groups and day 12 for the X-ray group), and at days 35, 70, and 105. For saliva sampling, pilocarpine (0.375 mg/kg, Pilocarpine hydrochloride, Sigma) was intraperitoneally administered to the mice under injection anaesthesia (Zoletil-mix: xylasin 20 mg/ml + butorphanol 10 mg/ml + Zoletil® (zolazepam 125 mg and tiletamin 125 mg)). Saliva was then collected into a cotton swab for 15 min, which was subsequently centrifuged for 7500 g at 4℃ for 2 min. The obtained saliva volume was measured and stored at -80℃ until cytokine analysis. Saliva volume measurements were used to assess salivary gland function, while saliva and blood serum samples were used for cytokine analysis (Fig. 6C). Termination of the experiments and euthanasia of the animals were

performed at day 105 after onset of fractionated irradiation using overdose of anaesthetics (Pentobarbitol, Exagon Vet®, Richter Pharma AG).

Tissue processing and staining

The major salivary glands (submandibular (SMG), sublingual (SLG) and parotid glands (PG)) were collected upon termination and fixed in 10% formalin for 24 h before undergoing dehydration and paraffin embedding. For staining with hematoxylin and eosin (HE), alcian blue (AB), Masson trichrome (MT), and immunofluorescent (IF) antibodies, tissue sections of 4, 5, 6, and 4 µm, respectively were cut (Leica RM2155 microtome) and placed on microscopy glass slides (Superfrost Plus, Thermo Fisher) before deparaffination and hydration. For detailed staining procedures of HE, AB, and MT staining, see Supplementary materials. After staining, all sections were dehydrated and mounted with xylene-based mounting medium (Pertex, Chemi-Teknik) or Fluoromount G DAPI (Southern Biotech) for IF sections. Histological images were acquired using a Nikon DS-Ri1 camera with a CFI Plan Fluor objective (magnification stated in figures) for all stains.

Analysis of salivary gland area and fibrotic area

For quantification of the total area of the salivary glands, overview images of MT-stained central sections of SMG and SLG were used and the total gland area was estimated by contouring the circumference of the total gland using ImageJ (NIH, USA). In the present study, there was a risk of incomplete dissection of PG due to its structure and anatomical location. Since this could affect our results, PG was not included in the MT staining and the subsequent tissue analysis. MT-stained sections were used to quantify the fibrotic area of the salivary glands, as previously described[50,56].

Immunofluorescence labelling and analysis

Antigen retrieval was performed on deparaffinised sections of SMG, and the following primary antibodies were incubated over night at 4℃: rabbit anti-MIST1 (polyclonal anti-BHLHA15, Atlas Antibodies, 1:500 dilution), rat-anti cytokeratin 19 (CK19) (TROMA-3, Sigma-Aldrich, 1 µg/mL). The secondary antibodies used were Alexa Fluor donkey-anti-rabbit IgG 488 and Alexa Fluor goat-anti-rat IgG 555. The slides were mounted and simultaneously stained with DAPI using Fluoromount G DAPI (Southern Biotech) for cell nuclei. IF-labelled images were acquired using a 20x objective, and five images were taken of each gland to obtain a representative view of the entire gland. The number of $MIST1^+$ nuclei and the total number of nuclei (all $DAPI^+$ nuclei) were counted using thresholding and particle analysis in ImageJ. Cell density was calculated using total number of nuclei relative to the field of view and presented as total nuclei/μm^2.

Cytokine analysis

Cytokine analysis of serum and saliva were performed using the custom made 11-Plex Luminex Mouse Discovery Assay kit (cat. no.: LXSAMSM-12, Bio-Techne Ltd, Abingdon, UK) including MIP-1α, KC, G-CSF, IFN-γ, IL-1α, IL-1b, IL-6, IL-12 p70, IP-10, TIMP-1 and TNF and recorded on a Luminex IS 200 instrument (Bio-Rad, Hercules, CA, USA). Both serum and saliva samples were thawed on ice, vortexed and spun down at 16 000 g for 5 min at 4 °C. The samples were diluted (serum 1:1 and saliva 2:1) with the RD1-W buffer (R&D Systems, Abington, UK). All data were processed through the integrated Bio-plex software manager (Version 6.2, Build 175, www.bio-rad.com/bioplexsoftware, Bio-Rad, Hercules, CA, USA). Total protein concentrations in saliva samples were measured in mg/ml using spectrophotometry (Absorbance 280 nm, NanoDrop 2000c, Thermo Fisher Scientific). The cytokine levels in saliva were adjusted to total protein concentration and presented as (pg of cytokine)/(mg of total protein).

Statistical analyses

Statistical analyses were performed using Prism 9 for Windows (Version 9.4.1, GraphPad Software, LLC). A significance level of 0.05 was used for all analyses, and the P-value for each test is stated in the relevant figure. Saliva volume differences and cytokine levels in saliva and serum were analysed using mixed-effect analysis with a Tukey's multiple comparisons test. Total gland area and fibrotic area differences were analysed using Kruskal-Wallis test with Dunn's multiple comparisons test. $MIST1^+$/total nuclei and cell density differences were assessed using one-way ANOVA with Tukey's multiple comparisons test. Mixed-effect analysis was used because of missing values due to mice being euthanized as they reached humane endpoints. Parametric tests were performed only when all groups passed the normality tests. No significant differences were observed between the two non-irradiated control groups, and the X-ray and proton controls were therefore merged in all analyses.

Data availability

Data is provided within the manuscript or supplementary information files.

Received: 20 March 2024; Accepted: 13 September 2024
Published online: 27 September 2024

References

1. Johnson, D. E. *et al.* Head and neck squamous cell carcinoma. *Nat. Rev. Dis. Primers* **6**(1), 92 (2020).
2. Sung, H. *et al.* Global cancer statistics 2020: GLOBOCAN estimates of incidence and mortality worldwide for 36 cancers in 185 countries. *CA Cancer J. Clin.* **71**(3), 209–249 (2021).
3. Siddiqui, F. & Movsas, B. Management of radiation toxicity in head and neck cancers. *Semin. Radiat. Oncol.* **27**(4), 340–349 (2017).
4. Barazzuol, L., Coppes, R. P. & van Luijk, P. Prevention and treatment of radiotherapy-induced side effects. *Mol. Oncol.* **14**(7), 1538–1554 (2020).

5. Chibly, A. M. *et al.* Salivary gland function, development, and regeneration. *Physiol. Rev.* **102**(3), 1495–1552 (2022).
6. Gunning, J., Limesand, K. Chronic phenotypes underlying radiation-induced salivary gland dysfunction. *J. Dent. Res.* 00220345241252396 (2024).
7. Villa, A., Connell, C. L., Abati, S. Diagnosis and management of xerostomia and hyposalivation. *Ther. Clin. Risk Manag.* 45–51 (2014).
8. De Felice, F., Cattaneo, C. G., Franco, P. Radiotherapy and systemic therapies: Focus on head and neck cancer. *Cancers (Basel)* **15**(17) (2023).
9. Byun, H. K. *et al.* Physical and biological characteristics of particle therapy for oncologists. *Cancer Res. Treat. Off. J. Korean Cancer Assoc.* **53**(3), 611–620 (2021).
10. Friborg, J., Jensen, K., Eriksen, J. *et al.* Considerations for study design in the DAHANCA 35 trial of protons versus photons for head and neck cancer. *Radiother. Oncol.* 109958 (2023).
11. Sio, T. T. *et al.* Intensity modulated proton therapy versus intensity modulated photon radiation therapy for oropharyngeal cancer: First comparative results of patient-reported outcomes. *Int. J. Radiat. Oncol. Biol. Phys.* **95**(4), 1107–1114 (2016).
12. Manzar, G. S. *et al.* Comparative analysis of acute toxicities and patient reported outcomes between intensity-modulated proton therapy (IMPT) and volumetric modulated arc therapy (VMAT) for the treatment of oropharyngeal cancer. *Radiother. Oncol.* **147**, 64–74 (2020).
13. Vitti, E. T., Kacperek, A., Parsons, J. L. Targeting DNA double-strand break repair enhances radiosensitivity of HPV-positive and HPV-negative head and neck squamous cell carcinoma to photons and protons. *Cancers (Basel)* **12**(6) (2020).
14. Vitti, E. T. & Parsons, J. L. The radiobiological effects of proton beam therapy: Impact on DNA damage and repair. *Cancers* **11**(7), 946 (2019).
15. Fontana, A. O. *et al.* Differential DNA repair pathway choice in cancer cells after proton- and photon-irradiation. *Radiother. Oncol.* **116**(3), 374–380 (2015).
16. Grosse, N. *et al.* Deficiency in homologous recombination renders Mammalian cells more sensitive to proton versus photon irradiation. *Int. J. Radiat. Oncol. Biol. Phys.* **88**(1), 175–181 (2014).
17. Szymonowicz, K., Krysztofiak, A., Linden, J. V. *et al.* Proton irradiation increases the necessity for homologous recombination repair along with the indispensability of non-homologous end joining. *Cells* **9**(4) (2020).
18. Lupu-Plesu, M. *et al.* Effects of proton versus photon irradiation on (lymph)angiogenic, inflammatory, proliferative and anti-tumor immune responses in head and neck squamous cell carcinoma. *Oncogenesis* **6**(7), e354 (2017).
19. Fujinaga, H. *et al.* Biological characteristics of gene expression features in pancreatic cancer cells induced by proton and X-ray irradiation. *Int. J. Radiat. Biol.* **95**(5), 571–579 (2019).
20. Nielsen, S. *et al.* Comparison of coding transcriptomes in fibroblasts irradiated with low and high let proton beams and cobalt-60 photons. *Int. J. Radiat. Oncol. Biol. Phys.* **103**(5), 1203–1211 (2019).
21. Wang, L. *et al.* Proton versus photon radiation-induced cell death in head and neck cancer cells. *Head Neck* **41**(1), 46–55 (2019).
22. Schniewind, I., Hadiwikarta, W. W., Grajek, J. *et al.* Cellular plasticity upon proton irradiation determines tumor cell radiosensitivity. *Cell Rep.* **38**(8) (2022).
23. Juvkam, I. S. *et al.* Proton compared to X-irradiation induces different protein profiles in oral cancer cells and their derived extracellular vesicles. *Int. J. Mol. Sci.* **24**(23), 16983 (2023).
24. Nielsen, S. *et al.* Proton scanning and X-ray beam irradiation induce distinct regulation of inflammatory cytokines in a preclinical mouse model. *Int. J. Radiat. Biol.* **96**(10), 1238–1244 (2020).
25. Luhr, A. *et al.* "Radiobiology of proton therapy": Results of an international expert workshop. *Radiother. Oncol.* **128**(1), 56–67 (2018).
26. Paganetti, H. Mechanisms and review of clinical evidence of variations in relative biological effectiveness in proton therapy. *Int. J. Radiat. Oncol. Biol. Phys.* **112**(1), 222–236 (2022).
27. Jones, B. Why RBE must be a variable and not a constant in proton therapy. *Br. J. Radiol.* **89**(1063), 20160116 (2016).
28. Ödén, J., DeLuca, P. M. Jr. & Orton, C. G. The use of a constant RBE= 1.1 for proton radiotherapy is no longer appropriate. *Med. Phys.* **45**(2), 502–505 (2018).
29. Sorensen, B. S. *et al.* Does the uncertainty in relative biological effectiveness affect patient treatment in proton therapy?. *Radiother. Oncol.* **163**, 177–184 (2021).
30. Sorensen, B. S. *et al.* Relative biological effectiveness (RBE) and distal edge effects of proton radiation on early damage in vivo. *Acta Oncol.* **56**(11), 1387–1391 (2017).
31. Sorensen, B. S. *et al.* Relative biological effectiveness of carbon ions for tumor control, acute skin damage and late radiation-induced fibrosis in a mouse model. *Acta Oncol.* **54**(9), 1623–1630 (2015).
32. Saager, M. *et al.* Determination of the proton RBE in the rat spinal cord: Is there an increase towards the end of the spread-out Bragg peak?. *Radiother. Oncol.* **128**(1), 115–120 (2018).
33. Paganetti, H. Relative biological effectiveness (RBE) values for proton beam therapy. Variations as a function of biological endpoint dose and linear energy transfer. *Phys. Med. Biol.* **59**(22), 419–472 (2014).
34. McNamara, A. L., Schuemann, J. & Paganetti, H. A phenomenological relative biological effectiveness (RBE) model for proton therapy based on all published in vitro cell survival data. *Phys. Med. Biol.* **60**(21), 8399–8416 (2015).
35. Eulitz, J. *et al.* Increased relative biological effectiveness and periventricular radiosensitivity in proton therapy of glioma patients. *Radiother. Oncol.* **178**, 109422 (2023).
36. Eulitz, J. *et al.* Predicting late magnetic resonance image changes in glioma patients after proton therapy. *Acta Oncol.* **58**(10), 1536–1539 (2019).
37. Bahn, E. *et al.* Late contrast enhancing brain lesions in proton-treated patients with low-grade glioma: Clinical evidence for increased periventricular sensitivity and variable RBE. *Int. J. Radiat. Oncol. Biol. Phys.* **107**(3), 571–578 (2020).
38. Peeler, C. R. *et al.* Clinical evidence of variable proton biological effectiveness in pediatric patients treated for ependymoma. *Radiother. Oncol.* **121**(3), 395–401 (2016).
39. Underwood, T. S. A. *et al.* Asymptomatic late-phase radiographic changes among chest-wall patients are associated with a proton RBE exceeding 1.1. *Int. J. Radiat. Oncol. Biol. Phys.* **101**(4), 809–819 (2018).
40. Kerns, S. L. *et al.* Normal tissue toxicity prediction: Clinical translation on the horizon. *Semin. Radiat. Oncol.* **33**(3), 307–316 (2023).
41. Zlygosteva, O., Juvkam, I. S., Arous, D. *et al.* Acute normal tissue responses in a murine model following fractionated irradiation of the head and neck with protons or X-rays. *Acta Oncol.* 1–7 (2023).
42. Rocchi, C., Barazzuol, L. & Coppes, R. P. The evolving definition of salivary gland stem cells. *NPJ Regen Med.* **6**(1), 4 (2021).
43. Aure, M. H., Konieczny, S. F. & Ovitt, C. E. Salivary gland homeostasis is maintained through acinar cell self-duplication. *Dev. Cell.* **33**(2), 231–237 (2015).
44. Ninche, N., Kwak, M., Ghazizadeh, S. Diverse epithelial cell populations contribute to the regeneration of secretory units in injured salivary glands. *Development* **147**(19) (2020).
45. Weng, P. L. *et al.* Limited regeneration of adult salivary glands after severe injury involves cellular plasticity. *Cell Rep.* **24**(6), 1464–1470 (2018).
46. Luitje, M. E. *et al.* Long-term maintenance of acinar cells in human submandibular glands after radiation therapy. *Int. J. Radiat. Oncol. Biol. Phys.* **109**(4), 1028–1039 (2021).

47. Jiang, M., Azevedo-Pouly, A. C., Deering, T. G. *et al.* MIST1 and PTF1 collaborate in feed-forward regulatory loops that maintain the pancreatic acinar phenotype in adult mice. *Mol. Cell. Biol.* (2016).
48. Mona, M. *et al.* MIST1, an inductive signal for salivary amylase in mesenchymal stem cells. *Int. J. Mol. Sci.* **20**(3), 767 (2019).
49. Wang, L. *et al.* Patterns of protein expression in human head and neck cancer cell lines differ after proton vs photon radiotherapy. *Head Neck* **42**(2), 289–301 (2020).
50. Zlygosteva, O. *et al.* Cytokine levels in saliva are associated with salivary gland fibrosis and hyposalivation in mice after fractionated radiotherapy of the head and neck. *Int. J. Mol. Sci.* **24**(20), 15218 (2023).
51. Schaue, D., Kachikwu, E. L. & McBride, W. H. Cytokines in radiobiological responses: A review. *Radiat. Res.* **178**(6), 505–523 (2012).
52. Razzaque, M. S. & Taguchi, T. Pulmonary fibrosis: Cellular and molecular events. *Pathol. Int.* **53**(3), 133–145 (2003).
53. Boneberg, E.-M. & Hartung, T. Molecular aspects of anti-inflammatory action of G-CSF. *Inflamm. Res.* **51**, 119–128 (2002).
54. Jasper, J. *et al.* Effect of G-CSF on oral mucositis and traumatic ulcers produced in the tongue of rats undergoing radiotherapy: clinical and histologic evaluation. *Oral Surg. Oral Med. Oral Pathol. Oral Radiol.* **122**(5), 587–596 (2016).
55. Juvkam, I. S., Zlygosteva, O., Arous, D. *et al.* A preclinical model to investigate normal tissue damage following fractionated radiotherapy to the head and neck. *J. Radiat. Res.* (2022).
56. Hanson, I., Juvkam, I. S., Zlygosteva, O. *et al.* TGF-β3 increases the severity of radiation-induced oral mucositis and salivary gland fibrosis in a mouse model. *Int. J. Radiat. Biol.* 1–10 (2024).

Acknowledgements

This work was funded by UiO Life Science at the University of Oslo under grant reference 2018/10221 and South-Eastern Norway Regional Health Authority under grant number 2019050.

Author contributions

I.S.J., O.Z.: methodology, investigation, formal analysis, data curation, visualisation, writing – original draft and editing. M.S.: methodology, investigation, writing – review and editing. B.S.S.: resources, writing – review and editing. H.C.D.A.: formal analysis, writing – review and editing. H.K.G., N.J.E., T.M.S. and E.M.: conceptualisation, methodology, resources, supervision, writing – review and editing.

Declarations

Competing interests

The authors declare no competing interests.

Additional information

Supplementary Information The online version contains supplementary material available at https://doi.org/10.1038/s41598-024-73110-7.

Correspondence and requests for materials should be addressed to E.M.